

# Age-related reduction in microcolumnar structure in area 46 of the rhesus monkey correlates with behavioral decline

Luis Cruz<sup>\*†</sup>, Daniel L. Roe<sup>‡</sup>, Brigita Urbanc<sup>\*</sup>, Howard Cabral<sup>§</sup>, H. E. Stanley<sup>\*</sup>, and Douglas L. Rosene<sup>\*†1</sup>

<sup>\*</sup>Center for Polymer Studies and Department of Physics, Boston University, Boston, MA 02215; <sup>†</sup>Department of Anatomy and Neurobiology, Boston University School of Medicine, Boston, MA 02118; <sup>‡</sup>Yerkes National Primate Research Center, Emory University, Atlanta, GA 30322; and <sup>§</sup>Department of Biostatistics, Boston University School of Public Health, 715 Albany Street, T4E, Boston, MA 02118

Contributed by H. E. Stanley, September 21, 2004

Many age-related declines in cognitive function are attributed to the prefrontal cortex, area 46 being especially critical. Yet in normal aging, studies indicate that neurons are not lost in area 46, suggesting that impairments result from more subtle processes. One cortical feature that is functionally important, but that has not been examined in normal aging because of a lack of efficient quantitative methods, is the vertical arrangement of neurons into microcolumns, a fundamental computational unit of the cortex. By using a density-map method derived from condensed-matter physics, we quantified microcolumns in area 46 of seven young and seven aged rhesus monkeys that had been cognitively tested. This analysis demonstrated that there is no age-related reduction in total neuronal density or in microcolumn width, length, or periodicity. There was, however, a statistically significant decrease in the strength of microcolumns, indicating microcolumnar disorganization. This reduction in strength was significantly correlated with age-related cognitive decline on tests of spatial working memory and recognition memory independent of the effect of age. Modeling demonstrated that random neuron displacements of  $\approx 30\%$  of a neuronal diameter ( $< 3 \mu\text{m}$ ) produced the observed reduction in strength. Hence, it is possible that, with changes in dendrites and myelinated axons, subtle displacements of neurons occur that alter microcolumnar structure and correlate with age-induced dysfunction. Therefore, quantitative measurement of microcolumnar structure may provide a sensitive morphological method to assay microcolumnar function in aging and other conditions.

minicolumns | density map | cerebral cortex | primate brain | modeling

In recent years, the conventional wisdom that there is significant loss of neurons in the cerebral cortex during normal aging has been challenged by evidence that neuron numbers largely are preserved in the cortex in the absence of neurodegenerative disease (1). The absence of compelling evidence for widespread neuronal loss in normal aging has necessitated a search for other brain changes to explain cognitive decline associated with senescence. A prominent but little-studied anatomical feature of the cortex is the vertical arrangement of neurons seen in cell stains under low magnification as vertical stripes. These arrangements have been called micro- or minicolumns, are composed of  $\approx 100$  neurons, and are  $\approx 30 \mu\text{m}$  in diameter (2, 3).

Neurons within a microcolumn receive common inputs, have common outputs, are interconnected, and may constitute a fundamental computational unit of the cerebral cortex (2, 4–7). The microcolumn has been shown to be disrupted under many different conditions, including Alzheimer's disease (AD), Lewy body dementia (LBD) (8), autism (9), dyslexia (10), and schizophrenia (11). To facilitate investigations of microcolumns, we developed a density-map method to quantify efficiently and reliably microcolumnarity in standard histological preparations of postmortem brains from humans and laboratory animals. We used this density-map method (8) to characterize the degree of

microcolumnarity in AD and LBD and further developed the method (12) by defining microcolumnar strength, width, length, periodicity, and distance between microcolumns. Of particular interest for normal aging was the observation that microcolumns were disrupted in LBD without an overall loss of neurons (8). Because current studies of normal aging show no widespread loss of cortical neurons (1), we have applied the density-map method to derive quantitative measures of microcolumnarity in young and aged monkeys and compared these measures across age and with measures of cognitive impairment.

## Methods

**Subjects.** Brain tissue was obtained from seven young adult (6.4–11.8 years; mean 8.5) and seven aged (24.7–32.9 years; mean 30.1) female rhesus monkeys that were part of an ongoing study of the effects of aging on cognitive function. Animals were obtained from the Yerkes National Primate Research Center (YNPRC) at Emory University and selected according to strict criteria that excluded monkeys with health or experimental histories that could affect the brain and cognitive function. Monkeys reach sexual maturity at  $\approx 5$  years of age and rarely live beyond 35, indicating a ratio of monkey to human age of  $\approx 1$  to 3 (13). Thus, young adults ages 5–12 years correspond to humans between 15 and 36 years old, and elderly monkeys between 20 and 30-plus correspond to humans between 60 and 90-plus years of age.

**Animal Procedures.** Monkeys were housed first at the YNPRC and then at the Boston University Medical Center. Both facilities are fully accredited by the Association for the Assessment and Accreditation of Laboratory Animal Care. All procedures were approved by the institutional animal care and use committees at both institutions and conformed to the National Institutes of Health's *Guide for the Care and Use of Laboratory Animals* (14) and *Public Health Service Policy on Humane Care and Use of Laboratory Animals* (15). All but two of the young monkeys were tested on a battery of cognitive tests to characterize learning and memory function (16). At the conclusion, monkeys were deeply anesthetized and killed by exsanguination during transcardial perfusion of the brain with fixative. Twelve monkeys were perfused with 4 liters of fixative containing 1% paraformaldehyde and 1.25% glutaraldehyde, and the other two were perfused with a fixative containing 4% paraformaldehyde. The brain was blocked, *in situ*, in the coronal stereotactic plane, and one

Abbreviations: AD, Alzheimer's disease; LBD, Lewy body dementia; DNMS, delayed non-match to sample test; DRST, delayed recognition span task; CII, cognitive impairment index; *W*, microcolumnar width; *P*, distance between microcolumns; *L*, length (vertical span) of microcolumns; *S*, strength of microcolumns; *T*, degree of microcolumnar periodicity.

<sup>†</sup>To whom correspondence should be addressed at: Center for Polymer Studies, Department of Physics, Boston University, 590 Commonwealth Avenue, Boston, MA 02215. E-mail: ccruz@bu.edu.

© 2004 by The National Academy of Sciences of the USA

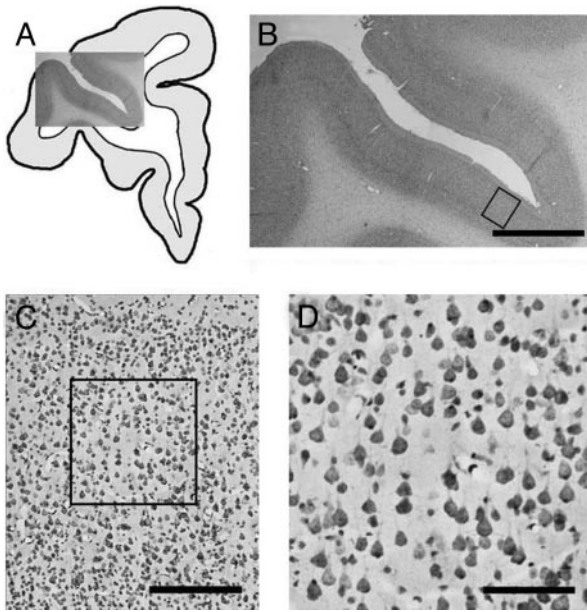


**Fig. 1.** Illustration of the level and site from which data were collected. (A) A camera lucida drawing of one hemisphere of the brain with a  $\times 1$  photomicrograph overlay of sulcus principalis. (B) A closeup of the overlay in A. The box along the lower bank, area 46, identifies the region of interest, shown at  $\times 10$  in C. D is a closeup of the boxed area from C, showing a  $512 \times 512$ -pixel area selected for analysis. Four such areas were analyzed per case. (Scale bars: 2.5 mm, 250  $\mu\text{m}$ , and 100  $\mu\text{m}$  for B, C, and D, respectively.)

hemisphere was cryoprotected in 20% glycerol and 2% DMSO in phosphate buffer (0.1 M, pH 7.4) and flash-frozen by immersion in  $-75^\circ\text{C}$  isopentane (17). All blocks were stored at  $-80^\circ\text{C}$  until cut.

**Tissue Processing.** Frozen blocks were cut in the coronal stereotaxic plane into eight interrupted series of 30- $\mu\text{m}$ -thick sections and one series of 60- $\mu\text{m}$ -thick sections so that sections in each series were spaced 300  $\mu\text{m}$  apart. One 30- $\mu\text{m}$ -thick series was stained with thionin. This cryoprotection and cutting procedure produces minimal shrinkage so that the  $(x,y,z)$  dimensions are largely preserved through the cutting procedure. Once cut and mounted, the sections adhere rapidly to the subbed surface of the slide before they dry, thus preserving the positional relationships within the  $x$ - $y$  plane of the section. However, as the section dries it shrinks in the  $z$  direction (thickness) from the originally cut thickness of 30  $\mu\text{m}$  to an average mounted section thickness of  $\approx 8$   $\mu\text{m}$  so that analysis of microcolumns is limited to the  $x$ - $y$  plane in this collapsed system.

**Cytoarchitectonic Regions Studied.** We selected area 46 of the prefrontal cortex in the lower bank of sulcus principalis for study. This neocortical region is implicated in working memory and executive functions (18–21), is easily identified, and provides a large area that is relatively flat and vertically oriented in coronal sections. We limited our analysis to layer III of area 46 because this layer is where cortico-cortical projections that subserve cortical information transfer originate. Because of this restriction, however, we cannot determine whether columnarity in other layers is affected to the same or a different extent as reported in this work.

**Digital Photography.** We selected sections from area 46 in the lower bank of the back third of the sulcus principalis (Fig. 1), according to architectonic criteria of Petrides and Pandya (22). We took photomicrographs with a digital camera at  $1,280 \times$

1,024 resolution spanning from the bottom of layer I through the top of layer IV at  $\times 10$  objective magnification on a Nikon E600 microscope and used the region containing layer III as input for a semiautomated neuron recognition.

**Semiautomated Detection of  $(x,y)$  Coordinates for Neurons.** We used a semiautomated neuron-detection method (12) to obtain  $(x,y)$  coordinates of neurons. Neurons are distinguished from glia and endothelial cells based on the relatively high optical density and the specific size of neuronal somas.

**Manual Identification of  $(x,y)$  Coordinates for Neurons and Glia.** For validation, we manually analyzed selected  $\times 10$  digital images by using the Bioquant (Nashville, TN) Image Analysis system and the  $\times 60$  objective to mark the  $(x,y)$  location of every neuron and every glia cell throughout the field of the  $\times 10$  image. As recently described (12), a comparison demonstrates that our semiautomated detection identifies at least 87% of neurons (SEM, 1.76%). Applying the density-map method to these manual coordinates demonstrated that there was no significant difference between microcolumnar measures derived from this method and the semiautomated method, i.e., the method is robust to the small, random underdetection of neurons that occurs with semiautomated detection (12).

**Density-Map Method and Microcolumnar Quantities.** The density-map method was initially described by Buldyrev *et al.* (8), and a more detailed description and validation is given by Cruz *et al.* (12). Briefly, the density map is a two-dimensional grayscale image in which different shades of gray are proportional to the average local neuronal density. By definition, the density map represents the average neuronal neighborhood surrounding a typical neuron within a region of interest. It follows from this description that the microcolumnar structure, if present, appears visually as one central vertical ridge, sometimes accompanied by two less pronounced neighboring (parallel) ridges. From the density map, the following quantities are derived (12):  $W$ , microcolumnar width;  $P$ , distance between microcolumns;  $L$ , length (vertical span) of microcolumns;  $S$ , strength of microcolumns (ratio of local neuronal density within a microcolumn to the total average neuronal density); and  $T$ , degree of microcolumnar periodicity (ratio of the neuronal density of neighboring microcolumns to the total average neuronal density).

Fig. 2A shows the average density map calculated by using as input all of the digitized images analyzed for the present work. As defined, local neuronal density is proportional to the level of darkness in the image so that the darkest parts have a higher local neuronal density than the background, revealing the central microcolumn with its two nearest parallel neighboring microcolumns. The white halo around the center depicts the size of the average diameter of a neuron and represents decreased neuronal density, because most neurons do not overlap due to mass exclusion. Fig. 2B is a closeup of Fig. 2A and shows the lengths  $P$ ,  $W$ , and  $L$  and the location where  $S$  and  $T$  are calculated.

**Neuron Modeling.** We modeled the effects of random neuron displacements on microcolumnar measures by first choosing as input experimental  $(x,y)$  data sets from one of the cases examined. In these simulations, we repeatedly subjected the  $(x,y)$  data set to random displacements with a random-walk algorithm in the fashion of Brownian motion. At each step, we changed each  $(x,y)$  neuron position by adding small increments  $(\delta x, \delta y)$ , which we took from a continuous random variable whose values ranged between  $-0.5$   $\mu\text{m}$  and  $0.5$   $\mu\text{m}$ . We then incremented each of the current new positions  $(x + \delta x, y + \delta y)$  by a new set of values  $(\delta x', \delta y')$ , and so on. Starting from the original  $(x,y)$  data set, we generated several new final sets with different numbers of total simulation steps ( $t$ ) = 25, 50, 75, 100, 125, 150, 200, 250, 300, 350,

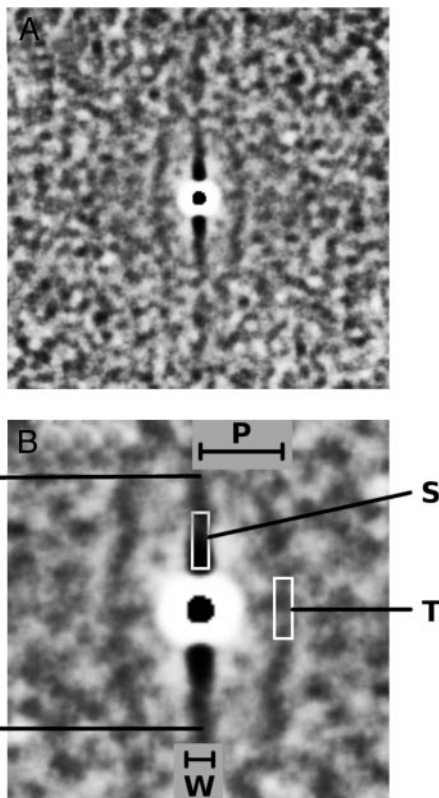


**Fig. 2.** Microcolumnar structure and local quantification. (A) The average density map for area 46, using as input neuron ( $x,y$ ) positions (14,080 neurons) from all of the cases analyzed. For visual clarity, we calculated this density map by placing identical disks of radius  $6\ \mu\text{m}$ , using as a center the ( $x,y$ ) neuron positions. (B) The central part of A in which we schematically define  $W$ ,  $L$ ,  $S$ , and  $T$ .  $W$ ,  $L$ , and  $P$  have units of length, whereas  $S$  and  $T$  are unitless and are defined as the ratio of the neuronal density found in the depicted white rectangles to the total neuronal density.

and 400. These final sets yielded configurations whose average displacements from the original locations were 1.86, 2.56, 3.13, 3.65, 4.07, 4.51, 5.17, 5.70, 6.15, 6.73, and  $7.19\ \mu\text{m}$ , respectively. To minimize variance in the estimates of displacement, we generated 10–50 sets for each input set as needed.

#### Behavioral Assessment of Young Adult and Aging Rhesus Monkeys.

All but two of the monkeys completed behavioral tests known to detect age-related cognitive impairments (16). One is the Delayed Non-Match to Sample test (DNMS), which evaluates rule-learning during acquisition and recognition memory when subsequently assessed over increasing temporal delays (2 min out to 10 min). The second, the Delayed Recognition Span Task (DRST), is a test of working memory capacity and is run in both a spatial and an object condition.

**Statistical Methods.** We examined individual parameters from our density-map analysis by using simple group comparisons and linear regression with a significance level of  $P \leq 0.05$  (two-tailed). For those density-map parameters that were significantly different between age groups, we then examined correlations between these parameters and behavioral measures to determine whether any observed alterations in microcolumnarity were associated with the age-related cognitive impairments. For this analysis, we set the significance level to  $P \leq 0.05$  (one-tailed) because we predicted that decreases in microcolumnar strength would correlate with age-related cognitive impairment.

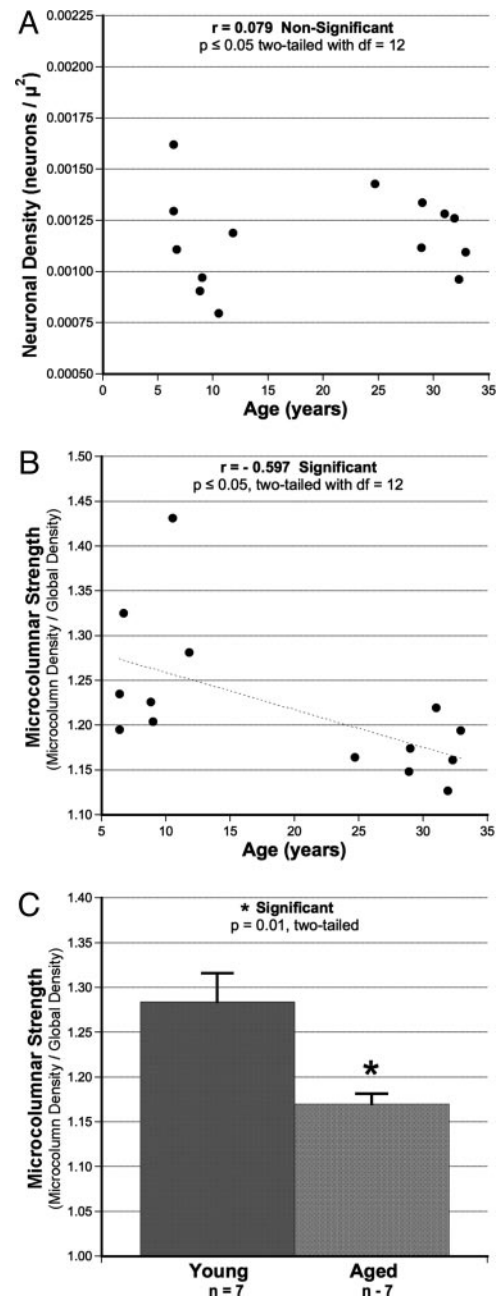


**Fig. 3.** Results of the effect of age on  $S$  despite lack of change in overall neuronal density. (A) Total neuronal density insensitive to age. (B) The age-related loss of microcolumnar strength ( $r = -0.597$ ;  $P \leq 0.05$ , two-tailed;  $df = 12$ ). (C) The significant reduction in  $S$  when subjects are grouped by age as young and old ( $P = 0.01$ ;  $df = 12$ ).

#### Results

**Microcolumnar Measures.** As shown in Fig. 3A, there was no overall effect of age on total neuronal density within the region of interest of the ventral bank of sulcus principalis. This observation is not surprising in light of accumulating evidence that neurons are not lost with age in area 46 (1, 23). Despite the preservation of neuronal density, there was a significant age-related reduction in  $S$  as a function of age in the scatter plot of Fig. 3B (Pearson correlation coefficient,  $r = -0.597$ ;  $P \leq 0.05$ ;  $df = 12$ ). As shown in Fig. 3C, this effect holds when the data are grouped as aged and young ( $P = 0.01$ ;  $df = 12$ ). In contrast to  $S$ , there was no effect of age on three other parameters of microcolumnar



54, there is a significant relationship between the decrease in  $S$  and the cognitive impairment index (CII) ( $r = 0.511$ ;  $P \leq 0.05$ , one-tailed;  $df = 10$ ). The CII is a composite of DNMS acquisition, DNMS 2-min delay, and DRST spatial span and, hence, is an overall assessment of cognitive impairment. Individual comparisons of  $S$  and each of the five individual behavioral measures indicate that there is a significant relationship between the decrease of  $S$  and lower scores on the DNMS 10-min delay test of recognition memory (Fig. 5B) ( $r = 0.563$ ;  $P \leq 0.05$ , one-tailed;  $df = 9$ ) and on the DRST spatial test of spatial working memory (Fig. 5C) ( $r = 0.660$ ;  $P \leq 0.01$ , one-tailed;  $df = 10$ ). The relationship between the decrease of  $S$  and initial acquisition of the DNMS task (a measure of rule learning) approached significance ( $r = 0.476$ ;  $P = 0.0085$ , one-tailed;  $df = 10$ ; data not shown).

Although these correlations are provocative, the strong effect of age on microcolumns and behavior raises the possibility that the relationship between a decrease in  $S$  and behavioral decline reflects only the effect of age. To control for this possibility, we used partial correlation methods to partial out the effect of age. Although doing this partial correlation analysis reduced the correlations between  $S$  and the CII ( $r = -0.27$ ;  $P = 0.20$ , one-tailed;  $df = 10$ ), significant or nearly significant relationships were still present between  $S$  and both the DNMS 10-min delay performance ( $r = 0.51$ ;  $P = 0.055$ , one-tailed;  $df = 10$ ) and the DRST performance ( $r = 0.54$ ;  $P = 0.036$ ;  $df = 10$ ).

## Discussion and Conclusions

**Summary of Results.** We used a density-map method from statistical physics to quantify microcolumnarity in layer III of area 46 in seven aged and seven young female rhesus monkeys. All of the aged and five of the young monkeys had completed a battery of cognitive tests. Our results demonstrate that there is a statistically significant reduction in  $S$  by nearly 40%  $\{[(1.28 - 1.0) - (1.17 - 1.0)] / (1.28 - 1.0) = 0.393\}$  in aged monkeys compared with young monkeys without any change in global neuronal density. This finding suggests a loss with age of the relative coherence of neurons within the statistically defined microcolumn. In contrast to this change in  $S$ , there was no age-related change in other measures of microcolumnarity that include  $W$ ,  $P$ , or  $T$ . A simulation demonstrated that an average random displacement from the detected position of neurons in layer III of as small as  $2.6 \mu\text{m}$  could produce the observed 40% reduction in  $S$ . Functionally, the reduction of  $S$  significantly correlated with an overall index of cognitive impairment (CII), a measure of spatial working memory (DRST), and recognition memory (DNMS 10 min), and approached significance on a measure of rule learning, the initial acquisition of the DNMS task.

**Technical Considerations.** Our semiautomated neuron detection method was validated in ref. 12 by manually marking positions of neurons in a sample of images and then comparing these two methods in two different ways. First, we compared the numbers of neurons detected and determined that we reliably detect  $\approx 87\%$  of the neurons identified manually. Second, we calculated the density maps by using both manually detected and semiautomated  $(x,y)$  locations for the same set of images. By comparing the quantitative measures of microcolumnarity, we confirmed that both density maps agree within error for  $L$ ,  $W$ ,  $P$ ,  $S$ , and  $T$ .

To minimize the effect that the curvature of tissue may have on the angular orientation of microcolumns, we limited our analysis to only the depth of the lower bank of sulcus where it is relatively flat and away from the extreme curvatures of the lip or fundus of any sulci. This limitation, of course, excludes from our calculations those regions that exhibit large variability in microcolumnar angular distributions as microcolumns “fan” out or in at tissue turns.

**Microcolumn Changes in the Adult Brain.** There are few other studies that have quantified microcolumns in the adult brain. Buldyrev *et al.* (8) used an earlier version of the density-map method to quantify microcolumns in subjects with AD and LBD. This study demonstrated a significant loss of microcolumnarity in  $L$  and  $W$  in both AD and LBD. Although some disruption of microcolumns in AD is not surprising given the overt cell loss, the change in LBD was surprising because there was no evidence of cell loss in these cases. Other methods that look at positional organization of neurons related to pathological conditions include early work by Benes and Bird (24), in which they applied computer-assisted stereomorphometric analyses to neuron  $(x,y)$  locations and found that the anterior cingulate cortex of schizophrenic patients may contain aggregates of neurons, particularly in layer II. Also, Urbanc *et al.* (25) used a crosscorrelation density-map method to study spatial relationships between the position and morphology of plaques with changes in neuronal architecture and revealed a focal neuronal toxicity associated with thioflavin S-positive plaque deposits in both AD and transgenic mice. Others, such as Casanova and Buxhoeveden, developed a method to quantify individually identified microcolumns, applying it to different human brain disorders (e.g., autism) (9–11, 27),<sup>||</sup> and to identify microcolumnar organization across species (28–29).<sup>\*\*</sup> Their method requires that sections be oriented so that visually observed microcolumns align vertically. Then, a Gaussian density distribution is calculated along the horizontal axis, and maxima are assumed to be the centers of microcolumns, although any that appear to be truncated are discarded (31). From visually confirmed individual microcolumns, many measures that are similar to ours are collected (e.g.,  $W$  and  $P$ ), but other quantities (e.g., cell spacing and the total path/length ratio) cannot be derived from our density map. The biggest difference is that their method measures the properties of all neurons in identified microcolumns, whereas our density-map method is a statistical average that considers every identified neuron in the region of interest. Thus, our density-map method has several advantages: (i) it only needs the  $(x,y)$  positions of the cells; (ii) it makes no assumptions about the presence, truncation, or orientation of microcolumns; (iii) slight imperfections are averaged out and do not significantly influence final quantities; (iv) it can be applied to any region, even those without any visually apparent microcolumnar organization; and (v) it provides two new quantities,  $S$  and  $T$ , that cannot be obtained easily by the alternative method. This last point is important in light of the results above, in which  $S$  may be a marker for the effects of age in different cortical regions.

**Mechanisms of Change in Microcolumnar Strength.** Our simulations demonstrate that isotropic random displacements as small as  $2.6 \mu\text{m}$  can produce the 40% reduction in microcolumnar strength observed here. However, other types of more specific randomizations also could play a role. For example, anisotropic movement along or perpendicular to the microcolumns that perturbs the interneuron distances (12) or horizontal displacements that might increase  $W$  also will decrease  $S$ . We note that because we treated all sections as simple two-dimensional planes, our simulations considered only  $(x,y)$  coordinates. Although a simulation of displacement in three-dimensional space could be done, it would not alter the conclusion that only small displacements can significantly alter  $S$ .

**Displacement of Neuron Location in Normal Aging.** If neuron loss is not the reason for the change in  $S$ , but, rather, neuron displace-

<sup>||</sup>Casanova, M. F., Buxhoeveden, D., Roy, E. & Switala, A. (2003) *Biol. Psychiatry* **53**, Suppl. S, 169 (abstr.).

<sup>\*\*</sup>Buxhoeveden, D. & Casanova, M. F. (2003) *Am. J. Phys. Anthropol.* **36**, 73 (abstr.).

